

# Low-field EPR studies of levels near the top of the barrier in Mn<sub>12</sub>-acetate reveal a new magnetization relaxation pathway

Boris Rakvin<sup>a,\*</sup>, Dijana Žilić<sup>a</sup>, Naresh S. Dalal<sup>b</sup>, Andrew Harter<sup>b</sup>, Yiannis Sanakis<sup>c</sup>

<sup>a</sup> Department of Physical Chemistry, Ruder Bošković Institute, P.O. Box 180, 10002 Zagreb, Croatia

<sup>b</sup> Department of Chemistry and Biochemistry, Florida State University, Tallahassee, FL 32306, USA

<sup>c</sup> Institute of Materials Science, NCSR 'Demokritos', Aghia Paraskevi Attikis, 15310 Athens, Greece

Received 7 February 2006; received in revised form 24 April 2006; accepted 7 May 2006 by D.D. Sarma

Available online 24 May 2006

## Abstract

We show that X-band electron paramagnetic resonance (EPR) measurements using a dual-mode resonance cavity can directly probe the levels near the top of the magnetization reversal barrier in the single-molecule magnet (SMM) Mn<sub>12</sub>-acetate. The observed transitions are much sharper than those reported in high-field EPR studies. The observed temperature dependence of the line positions points to the presence of a spin-diffusional mode. The correlation time for such fluctuations is of the order of  $6 \times 10^{-8}$  s at 10 K, and follows an Arrhenius activation energy of 35–40 K. These results open a new avenue for understanding the mechanism of tunneling and spin–lattice relaxations in these SMMs.

© 2006 Elsevier Ltd. All rights reserved.

PACS: 75.50.Xx; 75.60.Jk; 76.30.–v

Keywords: A. Mn<sub>12</sub>-Ac; E. EPR

## 1. Introduction

Mn<sub>12</sub>-acetate (henceforth Mn<sub>12</sub>-Ac) has been considered a very unusual material because it behaves as a magnet at a single-molecule level, exhibits a hysteresis loop under separated single-molecule conditions, and shows the novel phenomenon of magnetic quantum tunneling. Extensively studied over the last decade for showing this phenomenon, Mn<sub>12</sub>-Ac holds promise as a material for elements of magnetic memory devices at the molecular level [1–3]. We have performed electron paramagnetic resonance (EPR) spectroscopy of the magnetic levels near the top of the magnetization tunneling barrier in Mn<sub>12</sub>-Ac. These levels are most likely involved in the tunneling pathways and have not been studied before, most probably because the level separations fall in the low frequency X-band microwave region. Earlier studies [4] have suggested that the material is silent, i.e. not amenable to studies, at such low EPR frequencies of  $\sim 9.5$  GHz, at which most of the commercially available EPR spectrometers operate. Blinc et al. [5] showed that EPR

signals from Mn<sub>12</sub>-Ac could indeed be observed at the X-band frequencies, but they had to use more than one crystal to increase the detection sensitivity. In the present study, we successfully used high-Q and bimodal X-band cavities to study in detail the EPR transitions between the highest spin-energy levels, which may be a complement to the high-frequency techniques in characterizing Mn<sub>12</sub>-Ac and related materials.

Earlier high-field and high-frequency EPR studies have shown that such measurements provide a uniquely useful technique for characterizing the ground state spin-energy level scheme of Mn<sub>12</sub>-Ac [5–15]. It has been well established that Mn<sub>12</sub>-Ac (Mn<sub>12</sub>O<sub>12</sub>[(CH<sub>3</sub>COO)<sub>16</sub>(H<sub>2</sub>O)<sub>4</sub>]2CH<sub>3</sub>COOH·4H<sub>2</sub>O) [16] has an effective ground-state spin of  $S=10$  and strong crystal-field anisotropy. The anisotropy barrier blocks the magnetic moments along the easy axes of magnetization ( $z$ -axes) below the temperature of  $\sim 3.5$  K [1–3,11–15]. Magnetization relaxation and  $ac$ -susceptibility measurements have established that the barrier to magnetization reversal is about 65 K [1–3], but the exact details are still not fully understood [3]. Although dipolar interaction between different molecules is weak, this interaction could be essential for the understanding of magnetic quantum tunneling in the low temperature limit and near zero applied field. A high-field EPR spectroscopy study of the role of dipolar and exchange mechanism for the Mn<sub>12</sub>-Ac suggested that the temperature

\* Corresponding author. Fax: +385 1 468 0245.

E-mail address: [rakvin@irb.hr](mailto:rakvin@irb.hr) (B. Rakvin).

dependence of the EPR linewidths and line shifts was mainly caused by intermolecular spin–spin interactions (exchange and dipolar) and by the distribution of  $D$  and the  $g$  factor [11]. The monotonic line shifts observed for  $\text{Fe}_8\text{Br}$  were ascribed to a very small ( $\sim 10$  G) exchange interaction [11]. Unfortunately, such shifts were found to be rather small for  $\text{Mn}_{12}\text{-Ac}$  because the linewidths were much larger than the shifts [11]. Since the linewidths were  $M$ -dependent [11] and increased with applied magnetic fields, we anticipated that it might be advantageous to use low fields and frequencies, i.e. standard X-band frequencies, to measure such effects for  $\text{Mn}_{12}\text{-Ac}$ . In the present study, we used a dual-mode microwave cavity resonant in the X-band (9.5 GHz) region and observed several peaks, i.e. moderately strong EPR signals from the energy levels close to the top of the magnetization barrier in the temperature range from 40 K down to 10 K, when Boltzmann factors became unfavorable. These peaks have been discussed in terms of allowed and forbidden types of transitions ( $\Delta M = \pm 1, \pm 2, \pm 3, \pm 4$ ) resulting from a non-axial zero-field tensor, i.e. the  $E$  term in the spin Hamiltonian [1–3]. In particular, the peak positions were clearly and significantly temperature-dependent as opposed to the rather weak effect in the high-field EPR measurements [10]. In contrast to the case of  $\text{Fe}_8\text{Br}$  where a similar line-shift effect was ascribed to a small intermolecular exchange coupling, the line shifts found in this study have been ascribed to a magnetization diffusion mode, which could result from the slow (at EPR time scale of detection) rotational motion of the tilt of the magnetization axes of the various  $\text{Mn}_{12}\text{-Ac}$  isomers [17]. This is analogous to some earlier EPR spin-probe studies of ‘slow’ molecular motion in other non-magnetic materials [18–21]. Our study results yielded the motional correlation time and an Arrhenius activation energy barrier for this diffusional reorientational mode, whose definitive presence should be of considerable general interest in the single-molecule magnet (SMM) field.

## 2. Experimental

Single crystals of  $\text{Mn}_{12}\text{-Ac}$  were grown as described previously [7,8] according to the method of Lis [16]. The crystals were dark-violet rectangular parallel pipes, with the long dimensions along the easy magnetization axis. Their authenticity was checked via both  $ac$ - and  $dc$ - magnetization measurements, confirming the activation barrier and the total spin of  $S=10$  as well as the quantum steps in the hysteresis loops [1–3]. The crystal  $c$ -axis was the needle axis of the samples; hence sample alignment was relatively easy.

The EPR measurements were carried out with the standard X-band EPR spectrometer (Bruker Elexsys-500) equipped with ER 4122SHQE Super-High Q cavity and an Oxford continuous flow cryostat over 4–295 K. In addition to X-band system for spin-probe studies on  $\text{Mn}_{12}\text{-Ac}$ , which we had used in our previous work [22,23], in the present study we also used a Bruker 4116DM bimodal cavity that allowed us to orient the microwave magnetic field either parallel or perpendicular to the Zeeman field, as Piligkos et al. had done in their work [24]. The needle-shaped sample was positioned on the holder, so that

the plane of the rotation coincided approximately with the plane containing direction of magnetic field either parallel or perpendicular to the needle axis (along the global easy axis). Thus, the rotation plane was the crystal  $zx(y)$  plane. The largest uncertainty in the crystal orientation with respect to magnetic field was related to the optimal perpendicular deposition of the needle-shaped crystal to the crystal holder (within  $\pm 2^\circ$ ). The other rotation axis was controlled by a stepper-motor driven, programmable goniometer (Bruker, ER 218 PG1) with the accuracy of  $\sim 0.5^\circ$ . Powder spectra were obtained by gentle crushing of the crystals in vacuum grease to minimize any solvent loss. All computer simulations of the energy levels and EPR transitions were carried out with the Bruker XSophe program.

## 3. Results

### 3.1. X-band EPR spectra of $\text{Mn}_{12}\text{-Ac}$ and energy level diagram for expected transitions

Since this work involved the topmost energy levels of  $\text{Mn}_{12}\text{-Ac}$ , the energy-level diagram of the top levels was calculated as a function of the Zeeman field applied along the easy magnetization direction, the crystal  $c$ -axis (Fig. 1(a)). The spin Hamiltonian was calculated according to the following formula [1–3,10]:

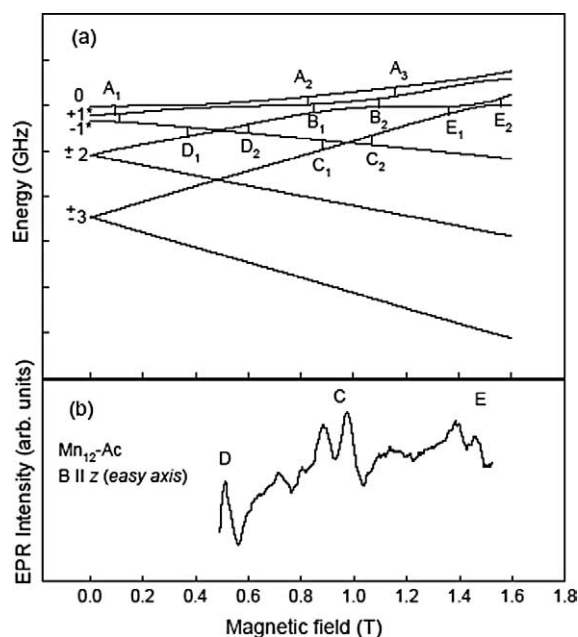


Fig. 1. (a) Energy level diagram of the top 4 ( $M=0, \pm 1, \pm 2, \pm 3$ ) levels of  $\text{Mn}_{12}\text{-Ac}$  for  $B||z$  (easy axis) by using the spin Hamiltonian parameters [6,10]. The solid arrows indicate the expected electron paramagnetic resonance transition at 9.35 GHz. (b) Observed electron paramagnetic resonance (EPR) X-band (9.35 GHz) spectra of  $\text{Mn}_{12}\text{-Ac}$  at 20 K. The spectrum is presented as first derivative of EPR spectrum detected at first harmonic of 100 kHz modulation frequency. Letters D, C, and E assign peaks with corresponding transitions.

$$\hat{H} = D \left( \hat{S}_z^2 - \frac{1}{3} \hat{S}(\hat{S} + 1) \right) + \mu_B \vec{B} \vec{g} \hat{S} + E \left( \hat{S}_x^2 - \hat{S}_y^2 \right) + B_4^0 \hat{O}_4^0 + B_4^4 \hat{O}_4^4, \tag{1}$$

where  $S_z$  is the projection of the spin operator  $\hat{S}$  along the  $z$ -axis and  $D$  is uniaxial anisotropy parameter. The second term in (1) is the Zeeman interaction and the remaining terms represent higher-order crystal field interactions. The accepted values of the spin Hamiltonian parameters,  $g_x = g_y = 1.94$ ,  $g_z = 2.0$ ,  $D = -0.454 \text{ cm}^{-1}$ ,  $E = \pm 0.002 \text{ cm}^{-1}$ ,  $B_4^0 = 2.0 \times 10^{-5} \text{ cm}^{-1}$ , and  $B_4^4 = \pm 3 \times 10^{-5} \text{ cm}^{-1}$  for  $\text{Mn}_{12}\text{-Ac}$  were taken from the earlier high-field EPR studies [6,10]. Clearly, the  $E$  term leads to level mixing and level crossings occur, leading to a complex set of doublets of peaks separated by an almost constant interval of the order of the  $D$  term. In our study, the lower  $M$  quantum number in the high-field limit for  $\vec{B}$  along the  $z$ -axis [6–8] is denoted by the subscripts to the letters A, B, C... in

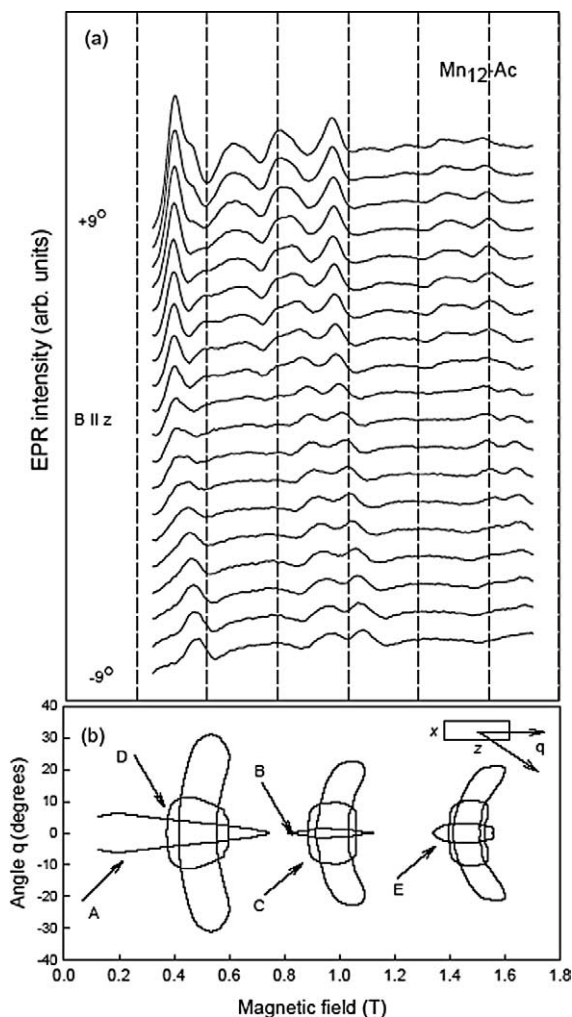


Fig. 2. (a) Observed angular dependence of the transitions in Fig. 1(a) for the Zeeman field  $\vec{B}$  in the  $z$ - $x$  ( $c$ - $a$ ) plane at 20 K. The field orientation is changed in  $1^\circ$  steps. The spectra are presented as first derivative of electron paramagnetic resonance spectra detected at first harmonic of 100 kHz modulation frequency. (b) Theoretical plot of the angular variation of the resonant fields of the transitions shown in Fig. 1(a).

Fig. 1. Fig. 1(b) shows a typical experimental spectrum, with the peak assignments according to Fig. 1(a). In addition, we verified that the transitions exhibited the angular dependence around the  $c$ -axis as expected from the high-field data on the higher  $M$  levels [6–8,10–14]. A typical set of spectra is shown in Fig. 2(a), together with calculated angular variation of the EPR transitions (shown in Fig. 1(a)) in the vicinity of easy axis (Fig. 2(b)). The expected series of doublets separated by about 0.4 T field is evident in Fig. 2(a), thus confirming the goodness of the parameter set.

Further confirmation of the peak assignment was obtained through the observation of some of the peaks in the so-called ‘parallel mode’ configuration, in which the microwave magnetic field is parallel to the Zeeman field [24]. Fig. 3 shows a comparison of the spectrum for  $\vec{B}$  along the  $z$ -axis in both the ‘parallel’ and ‘perpendicular’ modes, obtained by using the bimodal cavity. Albeit weaker due to a lower Q-factor, some of the normally ‘forbidden’ transitions ( $\Delta M = \pm 2, \pm 4$ ) in the investigated field range are seen at the expected positions, hence supporting the peak assignment.

There are three major groups of transitions located around the crossing of energy levels at applied magnetic field, as can be easily recognized in the vicinity of easy axis. From the complex transition map for  $S=10$ , only the high level transitions seem as possible EPR transitions (allowed EPR transition  $\Delta M = \pm 1$  in the vicinity of  $z$ -axis) in Fig. 1(a). However, for the low  $M$  value in the close vicinity of easy axis, the non-diagonal elements of the Hamiltonian (1) could significantly modify these energy levels. This modification can be easily verified from the monitored energy level diagram for  $\vec{B} \parallel z$  orientation at the zero field (Fig. 1(a)). All levels for higher values of  $\pm M$  are degenerated except for  $M = +1^*$  and  $M = -1^*$  states, which clearly show an amount of splitting proportional to the amount of rhombic parameter  $E$ . This suggests that other forbidden transitions ( $\Delta M = \pm 2$  and  $\pm 3$ ) become partly allowed and X-band EPR signal can be detected [25]. The presence of looping transition behavior in Fig. 2(b) is due to the presence of anti-crossing energy levels. Such anti-crossing levels are clearly resolved for  $M = \pm 1^*$  states in

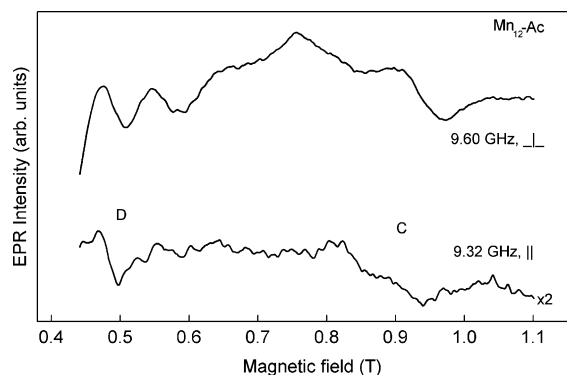


Fig. 3. Observed dual-mode electron paramagnetic resonance (EPR) X-band spectra of  $\text{Mn}_{12}\text{-Ac}$  for  $\vec{B} \parallel z$  at 18 K. Upper spectrum was recorded in the perpendicular-mode at 9.60 GHz of microwave frequency and lower spectrum is recorded in the parallel-mode at 9.32 GHz of microwave frequency. Letters D and C assign peaks with corresponding forbidden transitions.

energy levels graph (Fig. 1(a)). For example, the angular dependence of transition from  $M=1^*$  to  $M=0$ , marked by A in Fig. 2(b), is described by a loop that is wide along magnetic field scale and narrow along angular scale in the vicinity of  $z$ -axis. The transition denoted as B is presented by a loop that is narrower on magnetic field scale and wider on the angular scale than the loop A, and the further transition denoted by C is represented by a similar loop that is narrower along the magnetic field scale and wider along the angular scale than the second B loop (Fig. 2(b)). The EPR line expected for the A loop type transition exhibits high angular dependences, sudden disappearance, and gain in additional inhomogeneous broadening before the collapsing in the angular region where transition loop is nearly parallel to magnetic field (Fig. 2(b)). Thus, the line corresponding to transition A exhibits unusually high shift due to small change in the rotation angle (shift  $\sim 40$  mT for only one degree) in the close vicinity (a few degrees) of the  $z$ -axis. Since there are no indications for such behavior within the detected spectra in Fig. 2(a), it can be expected that the spectral lines related to A (the line with the highest expected intensity) mostly contribute to the background of the spectrum due to broad linewidth. In contrast, the C type transition in the near vicinity of 0.95 T shows a different angular dependence in the same angular interval. This transition exhibits narrower loop than the transitions A and B and results in a doublet of EPR lines (doublet splitting  $\sim 0.15$  T) in the particular angular interval (around  $\pm 10^\circ$  of the  $z$ -axis), as shown in Fig. 2(b). This doublet exhibits an angular dependence in the vicinity of easy axis similar to that of the detected spectra (Fig. 2(a)). This strongly supports the hypothesis that the detected resonant peak C at around 0.95 T is attributed to forbidden EPR transition from  $M=3$  to  $M=-1^*$ .

The spectra in Figs. 1(b) and 2(a) are presented in the first-derivative mode of the first harmonic of detection to obtain higher resolution necessary for the peak shift measurements. To study the temperature shift of the spectral lines, the spectrum with sharp peaks ( $\mathbf{B} \parallel z + 5^\circ$ ) was selected. The observed sharp EPR signals of this peak allowed us to measure the temperature dependence of the peak positions. We observed that every peak moved toward higher fields as the temperature increased (data not shown). Fig. 4(a) shows the temperature dependence of the part of the spectrum in the 10–30 K range. Fig. 4(b) shows the temperature dependence of the position of peak C. The visible characteristic shape suggested that a possible explanation could be a slow diffusional motional averaging model.

### 3.2. Spin diffusion model

We analyzed the temperature dependence using a spin diffusional model under the approximation of slow motion, i.e. the motion leading to the spectral changes was slow in comparison with the EPR time scale. For the superparamagnetic phase of SMM ( $T > T_B$ , where  $T_B \approx 65/\ln(t/\tau_0)$  K  $\approx 2.4$  K for  $t \approx 1$  h is blocking temperature), the appearance of magnetization relaxation rate is expected in the order of  $1/\tau$  (where  $\tau \sim 10^{-8} \times \exp(65/T)$  for  $\text{Mn}_{12}\text{-Ac}$ ) [26].

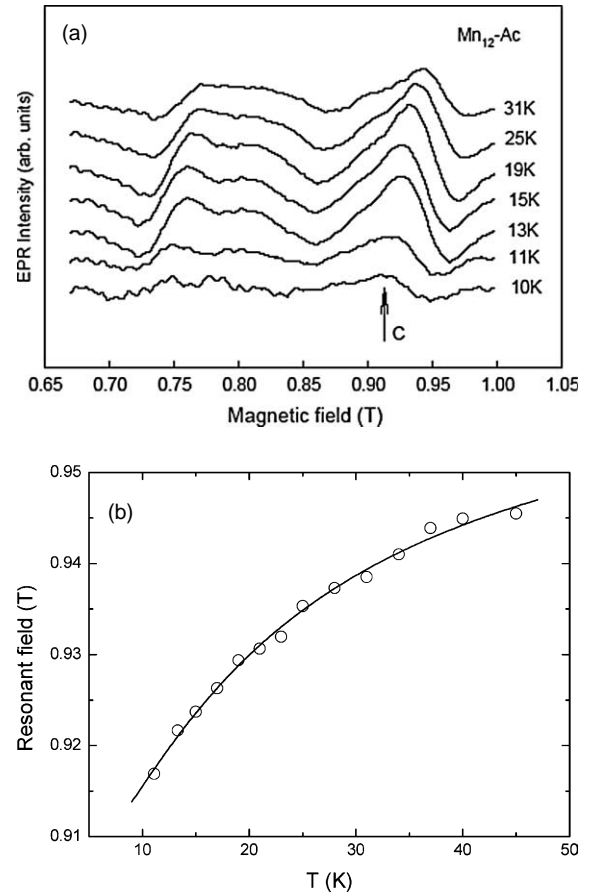


Fig. 4. (a) Temperature dependence of the electron paramagnetic resonance transitions for the magnetic field orientation along the  $z-5^\circ$  direction. The arrow denotes monitored peak C. (b) Experimentally measured temperature dependence of the resonance field for the transition C near 0.95 T (open circles). The full line presents the best-fitted data calculated from the non-linear fit of the relation (6) to experimental data.

The Arrhenius behavior of magnetization in the temperature region above  $T_B$  has been well established based on the  $ac$ -susceptibility experiments and is characterized by two distinct temperature regions. In the lower temperature region of 4–10 K, the low frequency  $ac$ -measurements ( $\sim 100$  kHz detection frequency) lead to comparable activation energy and pre-exponential factor of  $\tau_0$  as detected at low temperature by direct measurements of magnetization relaxation [26]. However, the  $ac$ -susceptibility experiments performed at high frequency ( $\sim 1$  MHz detection frequency) allow for measurements in the wider temperature interval (10–30 K), exhibit strong decrease in the preexponential factor ( $\tau_0 \sim 1 \times 10^{-12}$  s), and show increase in the activation energy ( $\Delta E \sim 160$  K) [27]. Since detection of a single EPR transition between two magnetic states appears in the GHz region, the fluctuation of magnetization at the several orders of magnitude slower rates can be treated as a slow spin diffusion process. Additionally, paramagnetic centers may be assumed to exhibit a small-angle slow orientational diffusion motion about external magnetic field  $\mathbf{B}$  along the easy axis. On the basis of this assumption, we may expect a slow diffusion averaging process for anisotropic paramagnetic center described by

fine-structure spin Hamiltonian (1). The rigid-limit fine-structure EPR spectra undergo pronounced changes in the line broadening at elevated temperatures and line shift depends on the averaging process described by  $\tau$ . In the present study, the analytical–theoretical treatment based on the solution of the isotropic orientational diffusion equation suggested by Lee et al. [18–21] was adapted to calculate slow motional dynamic line broadening and line shift of the simple EPR fine-structure centers [20]. On the basis of the spin–lattice Hamiltonian (1), where high-order crystal terms may be neglected, the linewidth broadening contribution expressed in the form of the spin–spin relaxation time,  $T_2$ , (described for transition  $M$  to  $M-1$ ) under slow isotropic spin diffusion  $\tau$  and magnetic field,  $\mathbf{B}$ , along the axial axis ( $z$ -axis) can be obtained as follows [20]:

$$\frac{1}{T_2^M(z)} = \left(\frac{1}{18}\right)^{1/2} \left\{ \frac{25\Delta_M^4 + 40\Delta_M^2\delta_M^2 + 16\delta_M^4}{2\Delta_M^2 + 2\delta_M^2} \right\}^{1/4} \tau^{-1/2}. \quad (2)$$

$$\begin{aligned} \Delta_M &= -\left(\frac{4\pi}{h}\right) \left[ \Delta g\mu_B B + \frac{3}{2}D(2M-1) \right] \\ \delta_M &= -\left(\frac{4\pi}{h}\right) \left[ \delta g\mu_B B + \frac{3}{2}E(2M-1) \right] \\ \Delta g &= \left[ g_z - \frac{g_x + g_y}{2} \right] \\ \delta g &= \frac{g_x - g_y}{2} \end{aligned} \quad (3)$$

The corresponding line-shift is given by the following formula:

$$|\Delta B^M(z)|_{sh} = 8^{-1/2} \left( \frac{h}{\pi g_z \mu_B} \right) \Delta_M \left[ \frac{2\Delta_M^2 + 2\delta_M^2}{25\Delta_M^4 + 40\Delta_M^2\delta_M^2 + 16\delta_M^4} \right]^{1/4} \times \tau^{-1/2} \quad (4)$$

The above equations for the  $\Delta M = \pm 1$  transitions show both the spectral line broadening and line shift depend on  $\tau^{-1/2}$  for the magnetic field oriented along the easy axis. This relationship is reminiscent of the time-square-root law predicted [28,29] for magnetization decay.

A qualitative conclusion from the above equations is that the temperature dependence of the linewidths and the line shifts yield direct information on the timescale of the underlying motion. Since  $\tau$  must decrease with an increase in temperature  $T$ , the lines should broaden and shift with an increase in  $T$ . For  $Mn_{12}$ -Ac, some degree of linebroadening can be seen in many high-field EPR spectra [10–14], but the analysis is complicated by inhomogeneous broadening due to the known  $g$ - and  $D$ -strain effects. Luckily, Mukhin et al. [30], who used the magnetic field-free variable frequency measurements on  $Mn_{12}$ -Ac, measured the temperature dependence of the linewidth for the ( $M = \pm 9$ ) line at  $8.5 \text{ cm}^{-1}$  (254.15 GHz), but did not discuss the underlying broadening mechanism in detail. Fig. 5 shows the experimental linewidth data they obtained [30] after converting the frequency into field units. Using the same

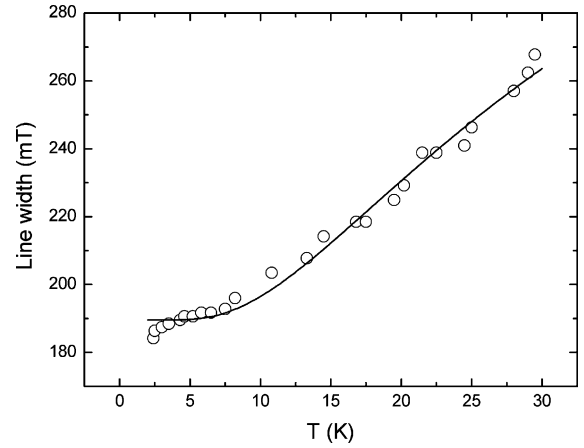


Fig. 5. Temperature dependence of linewidth (open circles) at half intensity of the transmission line ( $M = \pm 9$ ) for  $Mn_{12}$ -Ac detected by submillimeter transmission spectroscopy at  $8.5 \text{ cm}^{-1}$  (254.15 GHz) by Mukhin et al. [30]. The full line presents the best-fitted data calculated from the non-linear fit of the relation (5) to experimental data.

model and phenomenological extension of relation (2), we analyzed the data in Fig. 5, with the linewidth given by  $1/T_2$ , and assuming an Arrhenius behavior for the  $\tau$ :  $\tau = \tau_0 \exp(-\Delta E/kT)$ . This yielded the following Eq. (5)

$$\Gamma(T)_M = \Gamma_0 + \Gamma_M \exp(-\Delta E/2kT), \quad (5)$$

where  $\Gamma$  represented linewidth at half intensity. The experimental data were fitted into the Eq. (5) and corresponding parameters were obtained ( $\Delta E = 71 \pm 4 \text{ K}$ ,  $\Gamma_0 = 0.24 \pm 0.02 \text{ T}$ ,  $\Gamma_M = 0.191 \pm 0.001 \text{ T}$ ). The found activation energy of  $\sim 70 \text{ K}$  was close to the known magnetization reversal barrier of  $\sim 65 \text{ K}$ . However,  $\tau_0 \sim 1 \times 10^{-9} \text{ s}$  was about an order of magnitude shorter than that found by the  $ac$ -susceptibility method. Clearly, the barrier remained the same as expected, but different relaxation pathways started to emerge at different temperature as long as it was not too high. Our main conclusion from this fit is that the diffusional motion model yields reasonable results for  $Mn_{12}$ -Ac. The extension to  $T = 10 \text{ K}$  yields a  $\tau$  of  $1.2 \times 10^{-6} \text{ s}$ , which is also reasonable. It is to be noted here that we have assumed the spin Hamiltonian parameters, such as  $g$ ,  $D$ , and  $E$ , to be temperature independent. This is in agreement previous high-field EPR studies [10–14].

We then extended the model to line shifts. Again we used relation (4) and assumed the temperature independence of  $g$ ,  $D$ , and  $E$ , and the validity of the Arrhenius law for the correlation time  $\tau$ . Under these approximations, Eq. (4) can be recast as:

$$B(T)_{res}^M = B(0)_{res}^M + C_M e^{-\Delta E/2kT}. \quad (6)$$

This functional form can be smoothly fitted on the experimental results for measured high level EPR transitions (data shown in Fig. 4(b)). The peak used is the one marked C ( $M = 3$  to  $M = -1^*$ ) in Fig. 4(a). The obtained parameters from the fit are  $B(0)_{res}^0 = 0.907 \pm 0.003 \text{ T}$ ,  $C_3 = 0.061 \pm 0.002 \text{ T}$ , and  $\Delta E = 38 \pm 5 \text{ K}$ . The evaluated  $\Delta E$  exhibits smaller value than that measured by the  $ac$ -experiments ( $\Delta E \sim 65 \text{ K}$  in the low temperature region and  $\Delta E \sim 160 \text{ K}$  for high frequency  $ac$ -susceptibility measurements [26,27]). The constant  $C_3$  and

relation (4) are employed to estimate  $\tau_0 = 1.36 \times 10^{-9}$  s for the corresponding  $M=3$  level. The estimated  $\tau_0$  is of the same order of magnitude as  $\tau_0$  obtained for  $M=9$  level discussed above. On the other hand, the higher level exhibits faster dynamical fluctuation  $\tau = 6.1 \times 10^{-8}$  s at 10 K than the lower level state. This comparison strongly indicates that fluctuations of an individual spin state measured here differed from the magnetic fluctuations attributed to the average of all spin states detected by the ac-measurements. To verify the obtained  $\tau$ , the corresponding  $\Delta\Gamma = 0.0213$  T contribution of the linewidth broadening from measured shift at 10 K was recalculated. It can be noted that the obtained amount is significantly smaller than the experimentally measured  $\Gamma_3 \sim 0.9$  T linewidth at 10 K [11], indicating the expected small shift contribution as well as the advantage of line-shift measurements over direct linewidth measurements for broad inhomogeneous lines.

#### 4. Conclusion

We have shown that a dual-mode X-band EPR cavity system can provide important complementary information to the high-field techniques for probing the levels close to the magnetization reversal barrier in  $\text{Mn}_{12}\text{-Ac}$  and related systems. A significant advantage is that such techniques are available in almost every chemistry laboratory. The observed transitions are sharper because of the drastically reduced  $g$ - and  $D$ -strain broadening. The method should make the measurement of the transverse anisotropy parameter and its possible distribution rather easy. A recent study [31] has proposed that the distribution of  $E$  could be related to the magnetization relaxation in the SMMs. The present report might lead to further studies in this area.

#### References

- [1] G. Christou, D. Gatteschi, D.N. Hendrickson, R. Sessoli, *MRS Bull.* 25 (2000) 66.
- [2] D. Gatteschi, R. Sessoli, *Angew. Chem. Int. Ed.* 42 (2003) 268.
- [3] E. del Barco, A.D. Kent, S. Hill, J.M. North, N.S. Dalal, E.M. Rumberger, D.N. Hendrickson, N. Chakov, G. Christou, *J. Low Temp. Phys.* 140 (2005) 119.
- [4] A. Caneschi, D. Gatteschi, R. Sessoli, A.L. Barra, L.C. Brunel, M. Guillot, *J. Am. Chem. Soc.* 113 (1991) 5873.
- [5] R. Blinc, P. Cevc, D. Arčon, N.S. Dalal, R.M. Achey, *Phys. Rev. B* 63 (2001) 212401.
- [6] A.L. Barra, D. Gatteschi, R. Sessoli, *Phys. Rev. B* 56 (1997) 8192.
- [7] S. Hill, J.A.A.J. Perenboom, N.S. Dalal, T. Hathaway, T. Stalcup, J.S. Brooks, *Phys. Rev. Lett.* 80 (1998) 2453.
- [8] J.A.A.J. Perenboom, J.S. Brooks, S. Hill, T. Hathaway, N.S. Dalal, *Phys. Rev. B* 58 (1998) 330.
- [9] S. Maccagnano, R. Achey, E. Negusse, A. Lussier, M.M. Mola, S. Hill, N.S. Dalal, *Polyhedron* 20 (2001) 1441.
- [10] S. Hill, S. Maccagnano, K. Park, R.M. Achey, J.M. North, N.S. Dalal, *Phys. Rev. B* 65 (2002) 224410.
- [11] K. Park, M.A. Novotny, N.S. Dalal, S. Hill, P.A. Rikvold, *Phys. Rev. B* 65 (2002) 014426; K. Park, M.A. Novotny, N.S. Dalal, S. Hill, P.A. Rikvold, *Phys. Rev. B* 66 (2002) 144409; K. Park, M.A. Novotny, N.S. Dalal, S. Hill, P.A. Rikvold, *J. Appl. Phys.* 91 (2002) 7167.
- [12] E. del Barco, J.M. Hernandez, J. Tejada, N. Biskup, R. Achey, I. Rutel, N.S. Dalal, J. Brooks, *Phys. Rev. B* 62 (2000) 3018.
- [13] S. Hill, R.S. Edwards, S.I. Jones, N.S. Dalal, J.M. North, *Phys. Rev. Lett.* 90 (2003) 217204.
- [14] S. Takahashi, R.S. Edwards, J.M. North, S. Hill, N.S. Dalal, *Phys. Rev. B* 70 (2004) 094429.
- [15] E. del Barco, A.D. Kent, E.M. Rumberger, D.N. Hendrickson, G. Christou, *Europhys. Lett.* 60 (2002) 768.
- [16] T. Lis, *Acta Crystallogr. Sect. B* 36 (1980) 2042.
- [17] A. Cornia, R. Sessoli, L. Sorace, D. Gatteschi, A.L. Barra, C. Daiguebonne, *Phys. Rev. Lett.* 89 (2002) 257201.
- [18] D. Kivelson, S. Lee, *J. Chem. Phys.* 76 (1982) 5746.
- [19] S. Lee, D.P. Ames, *J. Chem. Phys.* 80 (1984) 1766.
- [20] S. Lee, S.-Z. Tang, *Phys. Rev. B* 31 (1985) 1308.
- [21] S. Lee, S.-Z. Tang, *Phys. Rev. B* 32 (1985) 2761.
- [22] B. Rakvin, D. Žilić, J.M. North, N.S. Dalal, *J. Mag. Res.* 165 (2003) 260.
- [23] B. Rakvin, D. Žilić, N.S. Dalal, J.M. North, P. Cevc, D. Arčon, K. Zadro, *Spectrochim. Acta A* 60 (2004) 1241.
- [24] S. Piligkos, D. Collison, V.S. Oganessian, G. Rajaraman, G.A. Timco, A.J. Thomson, R.E.P. Winpenny, E.J.L. McInnes, *Phys. Rev. B* 69 (2004) 134424.
- [25] J. Krzystek, J. Telsler, *J. Mag. Reson.* 162 (2003) 454.
- [26] B. Barbara, L. Thomas, F. Lioni, I. Chiorescu, A. Sulpice, *J. Magn. Magn. Mater.* 200 (1999) 167.
- [27] R. Blinc, B. Zalar, A. Gregorovič, D. Arčon, Z. Kutnjak, C. Filipič, A. Levstik, R.M. Achey, N.S. Dalal, *Phys. Rev. B* 67 (2003) 094401.
- [28] N.V. Prokofev, P.C.E. Stamp, *Phys. Rev. Lett.* 80 (1998) 5794.
- [29] N.V. Prokofev, P.C.E. Stamp, *J. Low. Temp. Phys.* 113 (1998) 1147.
- [30] A.A. Mukhin, V.D. Travkin, A.K. Zvezdin, S.P. Lebedev, A. Caneschi, D. Gatteschi, *Europhys. Lett.* 44 (1998) 778.
- [31] Z.D. Chen, S.Q. Shen, *Eur Phys. J. B* 48 (2005) 405.